PONTIFICIA UNIVERSIDAD CATÓLICA DEL PERÚ

ESCUELA DE POSGRADO

Non-collinear interaction of Laguerre-Gaussian modes in second harmonic generation

A thesis in candidacy for the degree of Master of Science in Physics presented by:

Jordy Guilbert Santiago Condori

Advisors:

Prof. Antonio Zelaquett Khoury
Universidade Fluminense Federal, Niterói-RJ, Brazil

Prof. Francisco de Zela
Pontificia Universidad Católica del Perú

Lima, 2018

ET LUX IN TENEBRIS LUCET
MCMXVII

Non-collinear interaction of Laguerre-Gaussian modes in second harmonic generation

Jordy Guilbert Santiago Condori

Propuesto para el grado de Magíster en Física

Resumen

Esta tesis aborda las interacciones no colineales de los modos Laguerre-Gaussianos. Estas interacciones se utilizan para lograr la transferencia del momento angular orbital (OAM) en la mezcla de ondas no lineales. Esto se hace mediante conmutación controlada por polarización .Ajustando la geometría de los haces de entrada, es posible producir una salida OAM de tres canales con cargas topológicas arbitrarias que se generan simultáneamente y se resuelven espacialmente en la longitud de onda del segundo armónico. El uso de grados de libertad de trayectoria y polarización permite una conmutación óptica casi perfecta entre las diferentes operaciones OAM. Se propone un modelo teórico que muestra un muy buena concordancia con los experimentos.

Non-collinear interaction of Laguerre-Gaussian modes in second harmonic generation

Jordy Guilbert Santiago Condori

Presented Towards a Master's Degree in Physics

Abstract

This thesis addresses non-collinear interactions of Laguerre-Gaussian modes. These interactions are used to achieve orbital angular momentum (OAM) transfer in non-linear wave mixing. This is done by polarization controlled switching. By adjusting the geometry of the input beams, it becomes possible to produce a three-channel, OAM-output with arbitrary topological charges that are simultaneously generated and spatially resolved in the second harmonic wavelength. The use of path and polarization degrees of freedom allows nearly perfect optical switching between diferent OAM operations. A theoretical model showing very good agreement with the experiments is proposed.

Acknowledgments

This thesis was possible thanks to a research stay during the months of March, April, May and June done in Niterói, Brazil. There, I had the opportunity to work in the Quantum Optics laboratory of the Universidade Federal Fluminense (UFF) under the supervision of the professor Antonio Zelaquett Khoury. I would like thank him for giving me this opportunity and supporting me during those months. Also, I thank the collaboration of Wagner Tavares Buono, his doctoral student, who guided me in the experimental part of this work.

I must express my very profound gratitude to the professor Francisco de Zela for giving me the suggestions that made possible the structure of this thesis and for making possible my research stay in Brazil.

A very especial grateful goes to my laboratory partners, especially to Piero Sánchez and Junior Gonzales, with whom I spent uncountable days trying to find countable photons and uncountable mistakes. I thank Yonny Yugra for his suggestions and recommendations as a friend and researcher.

For the scholarship I thank CIENCIACTIVA-CONCYTEC. I also believe that with science and technology our country will be a better one to live.

I thank my family: because I owe it all to you. They provided me unconditional support and continuous encouragement throughout my years of study and through the process of researching and writing this thesis. ¡Muchas gracias papá, mamá, Yvonne, David y Rodrigo!

And finally, last but by no means least, I thank each of my friends. Without our long conversations, my ideas about the universe and the life would be less exciting.

Escravos cardíacos das estrelas,
Conquistámos todo o mundo antes de nos levantar da cama;
Mas acordámos e ele é opaco,
Levantámo-nos e ele é alheio,
Saímos de casa e ele é a terra inteira,
Mais o sistema solar e a Via Láctea e o Indefinido.

Fernando Pessoa

Publications

Results contained in this Thesis have been published in the following article:

- W. T. Buono, J. Santiago, L. J. Pereira, D. S. Tasca, K. Dechoum, and A. Z. Khoury,*Polarization-controlled orbital angular momentum switching in nonlinear wave mixing*, Opt. Lett. **43** (2018), 1439-1442.

Contents

Chapter 1

Introduction

Since the invention of the laser, nonlinear optical effects have been gradually discovered, in part due to the high coherent light intensity that could be achieved. Thus, second harmonic generation was one of the first effects being discovered, in this case by Franken *et al* in 1961 [1]. Since then, second harmonic generation has been variously applied, among other things, to characterize materials [2, 3], for medical purposes [4, 5], and so on.

Moreover, experiments related to orbital angular momentum (OAM) in the second harmonic generation have been implemented and, as a result, topological charge doubling was demonstrated [6–8]. However, experiments performed with non-collinear interactions have not been intensively developed, so that just some few effects have been observed, such as non-conservation of angular momentum [9] or fractional OAM [10]. In this respect, a recent publication about non-collinear interactions of photons in second harmonic generation refers to a reduction in the conversion efficiency [11].

This thesis is an extension of the work done by Wagner et al. [25]; an extension that consists in the inclusion of an additional degree of freedom: the optical path. In the following chapters, we introduce some basic notions about nonlinear optics and, thereafter, we discuss second harmonic generation for cases in which we can control the degrees of freedom that are relevant to us: polarization, transversal mode and alignment.

Chapter 2

Introduction to nonlinear optics

Nonlinear optics studies the nonlinear response of materials, due to an applied electric field. As laser light can reach enough intensity to induce nonlinear responses in certain materials, the experimental exploration of nonlinear effects popped up after the construction of the laser by Maiman [12]. Albeit the beginning of nonlinear optics is commonly attributed to the experimental demonstration of second harmonic generation made by Franken*et al.* [1], some nonlinear optics effects had been already discovered before [13]. Second-order nonlinear optics, and particularly second harmonic generation, are in the focus of the present chapter.

2.1 Dielectric materials and polarization

Materials have different behaviors in response to an electric field. Dependent upon this response, materials are classified in three types: insulators or dielectrics, conductors, and semiconductors. We focus our attention on the response generated in dielectric materials which show high resistance, i.e., a poor response to an electric field. Thus, it is necessary to include "polarization" or dipole moment per unit volume $\vec{P}(\mathbf{r}, t)$ in order to characterize the orientation of the molecules in a material caused by an electric field. In this way, polarization affects the final electric field produced by the material, showing interesting optical effects under certain conditions of high intensity.

Let us start with Maxwell's equations [14]

$$\nabla \cdot \vec{D} = \rho \tag{2.1a}$$
$$\nabla \cdot \vec{B} = 0 \tag{2.1b}$$
$$\nabla \times \vec{E} = -\frac{\partial \vec{B}}{\partial t} \tag{2.1c}$$
$$\nabla \times \vec{H} = \frac{\partial \vec{D}}{\partial t} + \vec{J} \tag{2.1d}$$

Since we are working with dielectric materials, we may set

$$\rho = 0 \tag{2.2a}$$
$$\vec{J} = 0. \tag{2.2b}$$

As we mentioned above, $\vec{P}(\mathbf{r}, t)$ characterizes the material's response to an electric field. If we consider both the electric and magnetic responses, they are given by

$$\vec{B} = \mu_0 \vec{H} + \vec{M} \tag{2.3a}$$
$$\vec{D} = \epsilon_0 \vec{E} + \vec{P}. \tag{2.3b}$$

From (2.1c), (2.1b), (2.2a) and 2.3a we get, in the electric-dipole approximation,

$$\nabla \times \nabla \times \vec{E} + \mu_0 \frac{\partial^2}{\partial t^2} \vec{D} = 0. \tag{2.4}$$

Writing $\mu_0 = 1/\epsilon_0 c^2$ and applying

$$\nabla \times \nabla \times \vec{E} = \nabla(\nabla \cdot \vec{E}) - \nabla^2 \vec{E} \tag{2.5}$$

and taking $\nabla(\nabla \cdot E) = 0$ (under the slowly varying amplitude approximation), after inserting (2.3b) in (2.4) we get

$$\nabla^2 \vec{E} - \frac{1}{c^2} \frac{\partial^2}{\partial t^2} \vec{E} = \frac{1}{\epsilon_0 c^2} \frac{\partial^2 \vec{P}}{\partial t^2} \tag{2.6}$$

We can decompose $\vec{P}$ into a linear $\vec{P}^{(1)}$ and a nonlinear $\vec{P}^{NL}$ part:

$$\vec{P} = \vec{P}^{(1)} + \vec{P}^{NL}. \tag{2.7}$$

Similarly, we separate

$$\vec{D} = \vec{D}^{(1)} + \vec{P}^{NL} \tag{2.8}$$

where, according to (2.3b):

$$\vec{D}^{(1)} = \epsilon_0 \vec{E} + \vec{P}^{(1)} \tag{2.9}$$

The expression (2.6) gets then the form:

$$\nabla^2 \vec{E} - \frac{1}{\epsilon_0 c^2} \frac{\partial^2 \vec{D}^{(1)}}{\partial t^2} = \frac{1}{\epsilon c^2} \frac{\partial^2 \vec{P}^{NL}}{\partial t^2} \tag{2.10}$$

Considering an isotropic material, the relation between $\vec{D}$ and $\vec{E}$ is given by

$$\vec{D}^{(1)} = \epsilon_0 \epsilon^{(1)} \vec{E} \tag{2.11}$$

Finally, the electric field generated in a nonlinear material satisfies the equation

$$-\nabla^2 \vec{E} + \frac{\epsilon^{(1)}}{c^2} \frac{\partial^2 \vec{E}}{\partial t^2} = -\frac{1}{\epsilon_0 c^2} \frac{\partial^2 \vec{P}^{NL}}{\partial t^2} \tag{2.12}$$

$\epsilon^{(1)}$ relates with the refraction index $n(\omega)$ through the expression:

$$n(\omega) = (\epsilon^{(1)}(\omega))^{1/2} \tag{2.13}$$

2.2 Nonlinear susceptibility

In linear optics, the relation between electric field $E(t)$ and polarization $P(t)$ is simply given by

$$P(t) = \epsilon_0 \chi^{(1)} E(t), \tag{2.14}$$

where $x^{(1)}$ is the linear susceptibility and ϵ_0 is the permittivity of free space. In order to characterize the nonlinear behavior, we can develop $P(t)$ as a power series of $E(t)$:

$$\begin{aligned} P(t) &= \epsilon_0 \Big(\chi^{(1)} E(t) + \chi^{(2)} E^2(t) + \chi^{(3)} E^3(t) + ... \Big) \\ &= P^{(1)}(t) + P^{(2)}(t) + P^{(3)}(t) + ... \\ &= P^{(1)}(t) + P^{NL}(t) \end{aligned} \tag{2.15}$$

where $\chi^{(2)}, \chi^{(3)}$, etc., are nonlinear optical susceptibilities. $\chi^{(i)}$ represents mathematically an $i+1$-rank tensor. That is, we write more explicitly:

$$P_i = \epsilon_0 \Big(\chi^{(1)}_{ij} E_j + \chi^{(2)}_{ijk} E_j E_k + \chi^{(3)}_{ijkl} E_j E_k E_l + ... \Big) \tag{2.16}$$

To describe a nonlinear optical phenomenon, we use (2.12). In this case, on view of (2.15), the equation (2.12) reads

$$\nabla^2 E - \frac{n^2}{c^2}\frac{\partial^2 E}{\partial t^2} = \frac{1}{\epsilon_0 c^2}\frac{\partial^2 P^{NL}}{\partial t^2} \tag{2.17}$$

The term on the right-hand side of the above equation acts as a source of a non-homogeneous wave equation. It contains frequencies that are different from those of the incoming fields. Considering, for instance, an electric field containing two different frequencies:

$$E(t) = E_1 e^{-i\omega_1 t} + E_2 e^{-i\omega_2 t} + c.c. \tag{2.18}$$

The term corresponding to third-rank susceptibility in (2.15) reads

$$\begin{aligned} P^{(2)}(t) = \epsilon_0 \chi^{(2)}[E_1^2 e^{-2i\omega_1 t} + E_2^2 e^{-2i\omega_2 t} + 2E_1 E_2 e^{-i(\omega_1+\omega_2)t} \\ +2E_1 E_2^* e^{-i(\omega_1+\omega_2)t} + c.c.] + 2\epsilon_0 \chi^{(2)}[E_1 E_1^* + E_2 E_2^*], \end{aligned} \tag{2.19}$$

where each term in the above equation represents a second order phenomenon in nonlinear optics:

$$\begin{aligned} P(2\omega_1) &= \epsilon_0 \chi^{(2)} E_1^2 && \text{(SHG)} \\ P(2\omega_2) &= \epsilon_0 \chi^{(2)} E_2^2 && \text{(SHG)} \\ P(\omega_1 + \omega_2) &= 2\epsilon_0 \chi^{(2)} E_1 E_2 && \text{(SFG)} \\ P(\omega_1 - \omega_2) &= 2\epsilon_0 \chi^{(2)} E_1 E_2^* && \text{(DFG)} \\ P(0) &= 2\epsilon_0 \chi^{(2)}[E_1 E_1^* + E_2 E_2^*] && \text{(OR)} \end{aligned} \tag{2.20}$$

The above labels have the following meanings:

SHG: Second harmonic generation.
SFG: Sum frequency generation.
DFG: Difference frequency generation.
OR: Optical rectification.

On the other hand, if we deal with an electric field containing just a frequency ω, the expression (2.19) remains as

$$P^{(2)} = 2\epsilon_0 \chi^{(2)} E_1 E_1^* + (\epsilon_0 \chi^{(2)} E_1^2 e^{-i2\omega t} + c.c.) \tag{2.21}$$

where the first term does not contribute because of the second derivative in the equation (2.17). This contribution is also known as optical rectification and represents a static electric field produced in the nonlinear material. The second derivative term shows the doubled frequency that is responsible for second harmonic generation as we shall see in section 2.4.

2.3 Properties of the Nonlinear Susceptibility

A general expression for second order process in (2.16) is [18]

$$P_i(\omega) = \frac{1}{2}\epsilon_0 \sum_p \sum_{jk} \chi^{(2)}_{ijk}(\omega_3; \omega_1, \omega_2) E_j(\omega_1) E_k(\omega_2) \tag{2.22}$$

where $\omega_1 + \omega_2 = \omega_3$, and i, j, k can take on the values x, y and z. Addition over p means the sum over every permutation between ω_1 and ω_2. In principle, we need to compute all components χ_{ijk}. However, we may take into consideration some aspects to simplify the calculation of the susceptibility values:

2.3.1 Reality of the fields

In a lossless medium where frequencies are far from atomic and molecular resonances, the coefficients can be considered real [15]. As a consequence, we take account of negative frequencies as follows:

$$P(-\omega_n - \omega_m) = P^*(\omega_n + \omega_m), \tag{2.23}$$

$$E(-\omega_n) = E^*(\omega_n), \tag{2.24}$$

$$E(-\omega_m) = E^*(\omega_m). \tag{2.25}$$

Then, considering (2.22), susceptibility fulfils a similar condition:

$$\chi^{(2)}_{ijk}(-\omega_n - \omega_m, -\omega_n, -\omega_m) = (\chi^{(2)}_{ijk})^*(\omega_n + \omega_m, \omega_n, \omega_m). \tag{2.26}$$

2.3.2 Intrinsic Permutation Symmetry

The expression (2.22) contains products of two electric fields: $E_j(\omega_1)E_k(\omega_2)$. The order in which these fields appear in the sum can be interchanged, which implies that a possible antisymmetric part $\chi^{(A)}_{ijk}(\omega_n + \omega_m, \omega_n, \omega_m) = -\chi^{(A)}_{ikj}(\omega_n + \omega_m, \omega_m, \omega_n)$ would give no contribution to the sum. That is, $\chi^{(2)}_{ijk}$ can be assumed to have the

following intrinsic permutation symmetry:

$$\chi^{(2)}_{ijk}(\omega_n + \omega_m, \omega_n, \omega_m) = \chi^{(2)}_{ikj}(\omega_n + \omega_m, \omega_m, \omega_n) \tag{2.27}$$

2.3.3 Symmetries for Lossless Media

Indices can be exchanged fulfilling the energy conservation condition. So, for example, we have the equivalence:

$$\begin{aligned}\chi^{(2)}_{ijk}(\omega_3 = \omega_1 + \omega_2) &= \chi^{(2)}_{ijk}(\omega_1 = -\omega_2 + \omega_3) \\ &= \chi^{(2)}_{ijk}(\omega_2 = \omega_3 + \omega_1) \\ &= \chi^{(2)}_{ijk}(-\omega_1 = \omega_2 - \omega_3)\end{aligned} \tag{2.28}$$

2.3.4 Kleinman's symmetry

In addition, when the frequencies of the electric fields are lower than all resonant frequencies of the nonlinear material, the nonlinear susceptibility becomes independent of the frequency [16]. Thus, it is possible to permute indices i, j and k:

$$\begin{aligned}\chi^{(2)}_{ijk}(\omega_3 = \omega_1 + \omega_2) = \chi^{(2)}_{ijk}(\omega_1 = -\omega_2 + \omega_3) &= \chi^{(2)}_{ijk}(\omega_2 = \omega_3 - \omega_1) \\ \chi^{(2)}_{ijk}(\omega_3 = \omega_2 + \omega_1) &= \chi^{(2)}_{ijk}(\omega_1 = \omega_3 - \omega_2) \\ &= \chi^{(2)}_{ijk}(\omega_2 = -\omega_1 + \omega_3)\end{aligned} \tag{2.29}$$

2.3.5 Contracted Notation

Inserting the notation [18]

$$d_{ijk} = \frac{1}{2}\chi_{ijk} \tag{2.30}$$

and taking into consideration Kleinman's symmetry, we assume a free permutation between the last two indices. Therefore, we reduce the notation of d_{ij} to d_l, according to the table:

jk:	11	22	33	23,32	31,13	12,21
l:	1	2	3	4	5	6

Therefore, the susceptibility can be taken as a 3×6 matrix:

$$d_{il} = \begin{bmatrix} d_{11} & d_{12} & d_{13} & d_{14} & d_{15} & d_{16} \\ d_{21} & d_{22} & d_{23} & d_{24} & d_{25} & d_{26} \\ d_{31} & d_{32} & d_{33} & d_{34} & d_{35} & d_{36} \end{bmatrix}$$

This matrix multiplies a six-dimensional vector, whose first three components are $E_i(\omega_1)E_i(\omega_2)$, with $i = x, y, z$, while its last three components are given by $E_y(\omega_1)E_z(\omega_2)+E_y(\omega_2)E_z(\omega_1)$ plus two cyclic permutations thereof. Such a multiplication of matrix (d_{il}) with the six-dimensional vector gives then the polarization vector $P_{i=1,2,3}$.

Now, from Kleinman's symmetry, we get

$$d_{12} = d_{122} = d_{212} = d_{26} \tag{2.31}$$

and

$$d_{14} = d_{123} = d_{213} = d_{25}. \tag{2.32}$$

Our susceptibility, now, is much simpler:

$$d_{il} = \begin{bmatrix} d_{11} & d_{12} & d_{13} & d_{14} & d_{15} & d_{16} \\ d_{16} & d_{22} & d_{23} & d_{24} & d_{14} & d_{12} \\ d_{315} & d_{24} & d_{33} & d_{23} & d_{13} & d_{14} \end{bmatrix}$$

2.3.6 Effective value of d_{eff}

Selecting an appropriate geometry is viable to get a scalar susceptibility instead of a matrix for sum-frequency generation [18]:

$$P(\omega_3) = 4\epsilon_0 d_{eff} E(\omega_1)E(\omega_2) \tag{2.33}$$

Thus, in the second harmonic case($\omega_1 = \omega_2$) it is possible to write in a more compact way:

$$P(2\omega) = 2\epsilon_0 d_{eff} E^2(\omega), \tag{2.34}$$

where

$$E(\omega) = \left|\vec{E}(\omega)\right| = \Big[\sum_j E_j^2(\omega)\Big]^{\frac{1}{2}}. \tag{2.35}$$

Calculating d_{eff} in detail is beyond the scope of this thesis. For more information about how to compute d_{eff}, see Midwinter and Warner [17].
For our calculations in chapter 3 and 4, we will use the scalar expression of $\chi^{(2)}$.

2.4 Second harmonic generation

As it was mentioned before, second harmonic generation is a nonlinear phenomenon in which the initial beam is duplicated as a result of the interaction of two photons with the same frequency in a nonlinear material. However, second harmonic generation can exist only in a media without inversion symmetry, due to its odd anharmonic potential energy that is integrated over all space [18]. In this section, we deduce the intensity distribution and the phase matching conditions.

2.4.1 Amplitude equation

Proceeding as Ref. [18]. An electric field can be described by

$$E(t) = Ee^{-i\omega t} + c.c. \tag{2.36}$$

More specifically,

$$E_j(z,t) = E_j e^{-i\omega_j t} + c.c. \tag{2.37}$$

where we set

$$E_1 = A_1 e^{ik_1 z}\,(\text{Incident beam}), \tag{2.38}$$

$$E_2 = B_2 e^{ik_2 z}\,(\text{SHG beam}) \tag{2.39}$$

Using Kleinman's symmetry and replacing the susceptibility with its effective value, the expressions (2.34) and (2.33) become:

$$P_1(z) = 4\epsilon_0 d_{eff} E_2 E_1^* = 4\epsilon_0 d_{eff} B_2 A_1^* e^{i(k_2-k_1)z} \tag{2.40}$$

$$P_2(z) = 2\epsilon_0 d_{eff} E_1^2 = 2\epsilon_0 d_{eff} A_1^2 e^{2ik_1 z} \tag{2.41}$$

P_1 is the polarization caused by the incident electric field E_1 together with E_2, which originates under sum-frequency generation, while P_2 is the polarization caused by the amplified, incident electric field E_1. After including the respective temporal parts, we have

$$P_1(z,t) = P_1(z)e^{-i\omega_1 t} + c.c. \tag{2.42}$$

$$P_2(z,t) = P_2(z)e^{-i\omega_2 t} + c.c. \tag{2.43}$$

Equation (2.17) reads then as follows:

$$\frac{\partial^2 E_j(z,t)}{\partial z^2} - \frac{\epsilon^{(1)}(\omega_j)}{c^2}\frac{\partial^2 E_j(z,t)}{\partial t^2} = \frac{1}{\epsilon_0 c^2}\frac{\partial^2}{\partial t^2}P_j(z,t) \tag{2.44}$$

Inserting (2.43) and (2.37) in (2.44) for the case $j = 2$

$$\frac{d^2}{dz^2}(B_2 e^{i(k_2 z-\omega_2 t)}) - \frac{\epsilon^{(1)}(\omega_2)}{c^2}\frac{\partial}{\partial t^2}(B_2 e^{i(k_2 z-\omega_2 t)}) = \frac{1}{\epsilon_0 c^2}\frac{\partial^2}{\partial t^2}(2\epsilon_0 d_{eff} A_1^2 e^{i((2k_1)-\omega_2 t)}) \tag{2.45}$$

where we set $\frac{d^2}{dz^2}$ in place of ∇^2

$$\left[\frac{d^2 B_2}{dz^2} + 2ik_2\frac{dB_2}{dz} - k_2^2 B_2 + \frac{\epsilon^{(1)}(\omega_2)\omega_2^2 B_2}{c^2}\right] e^{i(k_2 z-\omega_2 t)} = \frac{-2d_{eff}\omega_2^2}{c^2} A_1^2 e^{i[(2k_1)z-\omega_2 t]} \tag{2.46}$$

and $k_2^2 = \epsilon^{(1)}(\omega_2)\omega_2^2/c^2$. We have dropped the complex-conjugate values and just kept the other terms. Then,

$$\left[\frac{d^2 B_2}{dz^2} + 2ik_2\frac{dB_2}{dz}\right] e^{i(k_2 z-\omega_2 t)} = \frac{-2d_{eff}\omega_2^2}{c^2} A_1^2 e^{i[(2k_1)z-\omega_2 t]} \tag{2.47}$$

As the amplitude increases slowly with z, we may use the approximation

$$\left|\frac{d^2 B_2}{dz^2}\right| \ll \left|k_2\frac{dB_2}{dz}\right| \tag{2.48}$$

Therefore,

$$\left[2ik_2\frac{dB_2}{dz}\right] e^{i(k_2 z-\omega_2 t)} = \frac{-2d_{eff}\omega_2^2}{c^2} A_1^2 e^{i[(2k_1)z-\omega_2 t]} \tag{2.49}$$

Finally, doing the same operations for the case $j = 1$, the amplitudes are ruled by the expressions

$$\frac{dA_1}{dz} = \frac{2i\omega_1^2 d_{eff}}{k_1 c^2} B_2 A_1^* e^{-i\Delta k z} \tag{2.50a}$$

$$\frac{dB_2}{dz} = \frac{i\omega_2^2 d_{eff}}{k_2 c^2} A_1^2 e^{i\Delta k z} \tag{2.50b}$$

with

$$\Delta k = 2k_1 - k_2 \tag{2.51}$$

2.4.2 Phase matching

From equations (2.50a) and (2.50b) one can see that whenever the so-called phase-matching condition

$$\Delta k = 0 \tag{2.52}$$

is satisfied, the energy transfer leading to second harmonic generation is more efficient. In order to achieve phase matching, it is necessary to know the polarization, the wavelength of the incident beams and the refractive index. We can have two kinds of phase matching: type I and II.

Type I is produced by the combination of two photons with the same polarization to generate a photon with twice the initial frequency. Type II consists in the combination of two photons with orthogonal polarizations in order to produce a photon with twice the initial frequency.

In our experiment, we have type II second harmonic generation, for which we employ a half wave plate (HWP). For type II second harmonic generation, equation (2.17) becomes:

$$\nabla^2 E_{2\omega} - \frac{n_{2\omega}^2}{c^2}\frac{\partial^2 E_{2\omega}}{\partial t^2} = \frac{\chi^{(2)}}{c^2}\frac{\partial^2 (E_\omega^H E_\omega^V)}{\partial t^2} \tag{2.53}$$

$E_{2\omega}$: Second harmonic electric field
E_ω^H : Incident horizontally polarized electric field
E_ω^V : Incident vertically polarized electric field

However, when the phase matching condition is not achieved, second harmonic beams have a lower intensity:

$$B_2(L) = \frac{id_{eff}\ \omega_2^2 A_1^2}{k_2 c^2}\int_0^L e^{i\Delta k z}dz = \frac{id_{eff}\omega_2^2 A_1^2}{k_2 c^2}\left(\frac{e^{i\Delta k L}-1}{i\Delta k}\right) \tag{2.54}$$

We integrate from 0 to L, where L is the transversal longitude of the nonlinear material. We consider that A_1 is independent of position [18]. The intensity of A_2 can be expressed as the time-averaged Poynting vector [14]

$$I_2 = 2n_2\epsilon_0 c|B_2|^2 \tag{2.55}$$

Adding in the equation (1.4.10)

$$\frac{2n_2\epsilon_0 d_{eff}\omega_2^4 A_1^4}{k_2^2 c^3}\left|\frac{e^{i\Delta k L}-1}{\Delta k}\right|^2 \tag{2.56}$$

$$\left|\frac{e^{i\Delta k L}-1}{\Delta k}\right|^2 = L^2\left(\frac{e^{i\Delta k L}-1}{\Delta k L}\right)\left(\frac{e^{-i\Delta k L}-1}{\Delta k L}\right) = 2L^2\frac{(1-\cos\Delta k L)}{(\Delta k L)^2}$$
$$= L^2\frac{\sin^2(\Delta k L/2)}{(\Delta k L/2)^2} \tag{2.57}$$

Putting A_1^2 in terms of the intensity, we obtain:

$$I_2 = \frac{2d_{eff}^2\omega_3^2 I_1^2}{n_1^2 n_2 \epsilon_0 c^2} L^2 \frac{\sin^2(\Delta kL/2)}{(\Delta kL/2)^2} \tag{2.58}$$

which gives us the intensity variation, see Fig. (2.1). Maximal intensity is obtained for $\Delta k \to 0$.

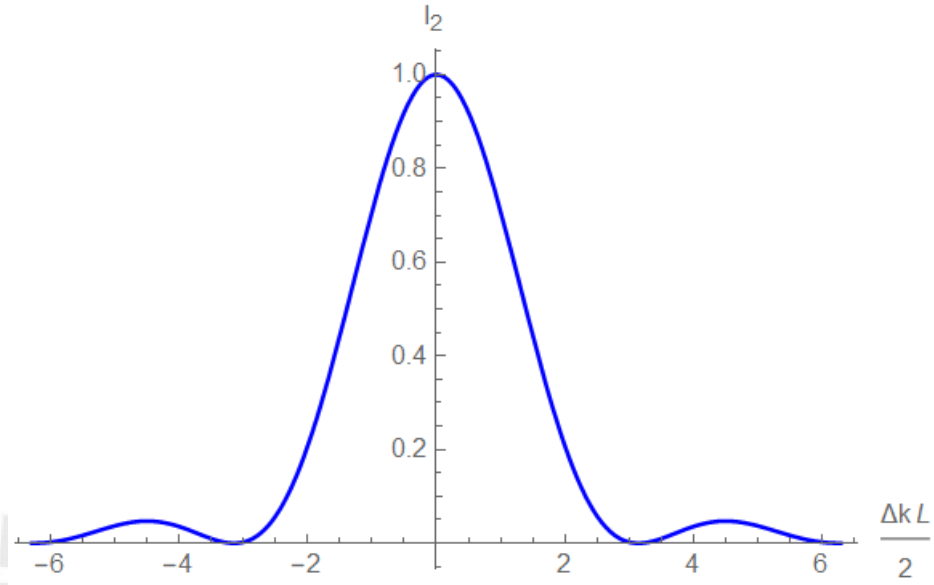

Figure 2.1: Transverse intensity profile of second harmonic generation

Chapter 3

Collinear interaction of Laguerre-Gaussian modes in second harmonic generation

In the last chapter we deduced the intensity distribution of the beams due to the effect of the second harmonic generation. In this chapter, we address similar issues but with the inclusion of orbital angular momentum.

3.1 Orbital angular momentum of light beams

We recall that the Poynting vector is defined by

$$\vec{S}(\vec{r},t) = c^2\epsilon_0[\vec{E}(\vec{r},t) \times \vec{B}(\vec{r},t)], \tag{3.1}$$

and the density of linear momentum by

$$\vec{p}(\vec{r},t) = \frac{\vec{S}(\vec{r},t)}{c^2} = \epsilon_0[\vec{E}(\vec{r},t) \times \vec{B}(\vec{r},t)], \tag{3.2}$$

which integrated over all space gives us the total linear momentum

$$\vec{P}(\vec{r},t) = \epsilon_0 \int_V [\vec{E}(\vec{r},t) \times \vec{B}(\vec{r},t)]dv \tag{3.3}$$

Similarly, the density of angular momentum is

$$\vec{l}(\vec{r},t) = \vec{r} \times \vec{p}(\vec{r},t) = \vec{r} \times \epsilon_0[\vec{E}(\vec{r},t) \times \vec{B}(\vec{r},t)] \tag{3.4}$$

and its integral over all space gives the total angular momentum

$$\vec{L} = \epsilon_0 \int_V \vec{r} \times [\vec{E}(\vec{r},t) \times \vec{B}(\vec{r},t)]dv \tag{3.5}$$

Replacing $\vec{B}$ by $\vec{\nabla} \times \vec{A}$, we have

$$\vec{L} = \epsilon_0 \int_V \vec{r} \times [\vec{E}(\vec{r},t) \times (\vec{\nabla} \times \vec{A}(\vec{r},t))]dv \tag{3.6}$$

and computing the cross product

$$[\vec{r} \times \vec{E} \times \vec{\nabla} \times \vec{A}]_p = -\epsilon_{pqi} r_q E_j (\partial_j A_i) + \epsilon E_j r_q \partial_i A_j \tag{3.7}$$

and solving with the conditions $\nabla \cdot E = 0$ and $\partial_i r_i = \delta_i^j$ (Kronecker delta):

$$\begin{aligned} \epsilon_{pqi} r_q E_j (\partial_j A_i) &= \epsilon_{pqi} \partial_j (r_q E_j A_i) - \epsilon_{pqi} r_q (\partial_j E_j) A_i - \epsilon_{pqi} (\partial_j r_q) E_j A_i \\ &= \epsilon_{pqi} \partial_j (r_q E_j A_i) - \epsilon_{pqi} E_q A_i. \end{aligned} \tag{3.8}$$

In this way, the total angular momentum reduces to

$$\begin{aligned} \vec{L} &= \epsilon_0 \int_V \Big[(\vec{E} \times \vec{A}) - \vec{\nabla} \cdot \vec{E} (\vec{r} \times \vec{A}) + E_i (\vec{r} \times \vec{\nabla}) A_i \Big] dv \\ &= \epsilon_0 \int_V \Big[(\vec{E} \times \vec{A}) + E_i (\vec{r} \times \vec{\nabla}) A_i \Big] dv + \oint_S \vec{E} (\vec{r} \times \vec{A}) \cdot ds \end{aligned} \tag{3.9}$$

Finally, integrating over all space, the last term vanishes. Thus, we can split the total angular momentum in two parts:

$$\vec{L} = \vec{L}_s + \vec{L}_o, \tag{3.10}$$

with

$$\vec{L}_s = \epsilon_0 \int_V \vec{E}(\vec{r},t) \times \vec{A}(\vec{r},t) dv \tag{3.11}$$

$$\vec{L}_o = \epsilon_0 \int_V E_i(\vec{r},t) \Big[\vec{r} \times \vec{\nabla} \Big] A_i(\vec{r},t) dv \tag{3.12}$$

where L_s represents spin, i.e., a property that is independent of position, and L_o represents an angular momentum that depends on the spatial distribution of the field. While L_s represents a space-independent property of the field, L_o can be controlled with a spatial light modulator (SLM). A detailed procedure is developed in [32]

3.2 Paraxial wave equation

In this part, we present some examples of spatial distribution of the electric field. Later, we use one of these solutions to exhibit the properties in the second harmonic that are due to the addition of transversal modes. From equations (2.1a)-(2.1d) we can deduce the wave equation when $\vec{J} = 0$ and $\rho = 0$. We get

$$\nabla^2 \vec{E} - \frac{1}{c^2}\frac{\partial^2 \vec{E}}{\partial t^2} = 0 \tag{3.13}$$

and

$$\nabla^2 \vec{B} - \frac{1}{c^2}\frac{\partial^2 \vec{B}}{\partial t^2} = 0 \tag{3.14}$$

We shall describe our electric field with a polarization and a transversal function:

$$\vec{E} = \psi(\vec{r})e^{i(kz-\omega t)}\hat{u}, \tag{3.15}$$

where $\hat{u}$ is the polarization and $\psi(\vec{r})$, the transversal function.
Inserting 3.15 in 3.13 we get

$$\begin{aligned}
&\nabla^2[\psi(\vec{r})e^{i(kz-\omega t)}] - \frac{1}{c^2}\frac{\partial^2 \psi(\vec{r})e^{i(kz-\omega t)}}{\partial t^2} = 0 \\
&= \left(\nabla^2[\psi(\vec{r})] + 2\vec{\nabla}[\psi(\vec{r})]\cdot\vec{\nabla}[e^{ikz}] + \psi(\vec{r})\nabla^2[e^{ikz}]\right)e^{-i\omega t} + k^2\psi(\vec{r})e^{i(kz-\omega t)} \\
&= \left(\nabla^2[\psi(\vec{r})] + 2ik\hat{z}\cdot\nabla[\psi(\vec{r})]\right)e^{i(kz-\omega t)} \\
&= 0
\end{aligned} \tag{3.16}$$

Hence, it holds

$$\nabla^2[\psi(\vec{r})] + 2ik\hat{z}\cdot\vec{\nabla}[\psi(\vec{r})] = 0. \tag{3.17}$$

We have assumed that there is a slow variation in the propagation direction. In addition, we assume the paraxial approximation [33]

$$\left|\frac{\partial^2\psi}{\partial z^2}\right| \ll \left|\frac{\partial^2\psi}{\partial x^2}\right|, \left|\frac{\partial^2\psi}{\partial y^2}\right| \text{ and } 2k\left|\frac{\partial\psi}{\partial z}\right| \tag{3.18}$$

which gives us

$$\nabla_\perp^2\psi + 2ik\frac{\partial\psi}{\partial z} = 0, \tag{3.19}$$

where $\nabla_\perp^2\psi$ stands for

$$\nabla_\perp^2\psi = \frac{\partial^2\psi}{\partial x^2} + \frac{\partial^2\psi}{\partial y^2}, \tag{3.20}$$

Equation (3.19) is known as the Helmholtz equation.

3.2.1 Gaussian modes

Equation (3.19) admits the following solution [21]:

$$\psi_0(x,y,z) = \sqrt{\frac{2}{\pi}}\frac{1}{w(z)}\exp\left[-\frac{x^2+y^2}{w^2(z)} + ik\frac{x^2+y^2}{2R(z)} - i\arctan\left(\frac{z}{z_R}\right)\right], \tag{3.21}$$

which is the most simple solution. The beam width $w(z)$ and wavefront radius $R(z)$ at position z are given by

$$w(z) = w_0\sqrt{\left(1+\frac{z_R^2}{z^2}\right)}, \tag{3.22}$$

$$R(z) = z\left(1+\frac{z_R^2}{z^2}\right). \tag{3.23}$$

z_R is called Rayleigh distance and is defined by the expression

$$z_R = \frac{\pi w_0^2}{\lambda} \tag{3.24}$$

3.2.2 Hermitte-Gaussian mode

When (3.19) is solved in Cartesian coordinates, we obtain as solutions Hermite-Gaussian modes:

$$\begin{aligned}\psi_{n,m}(x,y,z) = \frac{A_{mn}}{w(z)}H_n\left(\sqrt{2}\frac{x}{w(z)}\right)H_m\left(\sqrt{2}\frac{y}{w(z)}\right)\\ \times\exp\left[-\frac{x^2+y^2}{w^2(z)} + ik\frac{x^2+y^2}{2R(z)-i\phi_{mn}(z)}\right]\end{aligned} \tag{3.25}$$

A_{mn} is a normalization constant, H_m is the Hermite polynomial of order m [19], and $\phi_{mn}(z)$ is known as the Gouy phase, which reads as follows:

$$\phi_{mn}(z) = (m+n+1)\arctan\left(\frac{z}{z_R}\right) \tag{3.26}$$

The order of the Hermite-Gaussian mode is given by $N = m+n$. A particular case of a Hermite-Gaussian mode is a simple Gaussian mode, given by 3.2 with $m = 0$ and $n = 0$.

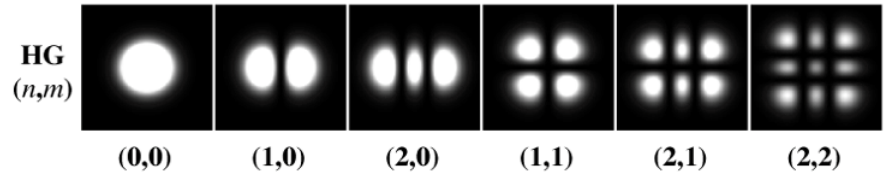

Figure 3.1: Intensity profile of Hermite-Gaussian modes [23]

3.2.3 Laguerre-Gaussian modes

When (3.19) is solved in cylindrical coordinates, we obtain as solutions the Laguerre-Gaussian modes.

$$\psi_p^l(\rho,\phi,z) = \frac{A_p^l}{w(z)}\left(\frac{\sqrt{2}\rho}{w(z)}\right)^{|l|} L_p^{|l|}\left[\frac{2\rho^2}{w^2(z)}\right]\exp\left[-\frac{\rho^2}{w^2(z)}\right] \times \exp\left[ik\frac{\rho^2}{2R(z)} + il\phi - i\phi_{pl}(z)\right]. \tag{3.27}$$

A_p^l is a normalization factor, $L_p^{|l|}$ is a general Laguerre polynomial [20] and ϕ_{pl} is the Gouy phase:

$$\phi_{pl}(z) = (2p + |l| + 1)\arctan\left(\frac{z}{z_R}\right) \tag{3.28}$$

By definition, the order of a Laguerre-Gaussian is $N = 2p + |l|$. The parameter p is known as radial charge and represents the number of rings in the transversal mode. The parameter l is called topological charge. It is a measure for the size of the rings in the transversal mode.

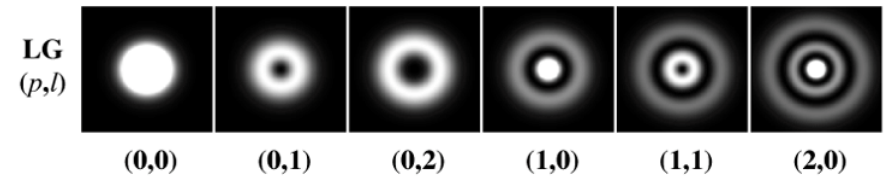

Figure 3.2: Intensity profile of Laguerre-Gaussian modes [23]

We notice that it is possible to go from Hermite-Gaussian modes to Laguerre-Gaussian modes and viceversa, as both of them are bases [22]. We can exhibit experimentally this equivalence, as discussed in chapter 6.

3.3 Vector beams

Until now, we have assumed a single polarization for a transversal mode; however, polarization can be different in every position of a combination of transversal modes.

This is known as a vector beam, which can be generally represented by

$$E_\omega(r,t) = \frac{1}{\sqrt{2}}(u_{lp}(r)\hat{\mathbf{e}}_{pol} + e^{i\phi}u_{l'p'}(r)\hat{\mathbf{e}}_{pol}). \tag{3.29}$$

Here, $\hat{\mathbf{e}}_{pol}$ is the polarization and $u_{lp}(r)$ is the transversal mode. In this way, we describe a family of vector beams for each type of transversal mode.
For Hermite-Gaussian beams, we have the following expression:

$$E_\omega(r,t) = \frac{1}{\sqrt{2}}(HG_{1,0}\hat{\mathbf{e}}_H + e^{i\phi}HG_{0,1}\hat{\mathbf{e}}_V). \tag{3.30}$$

The corresponding electric field intensities appear as in the following figure:

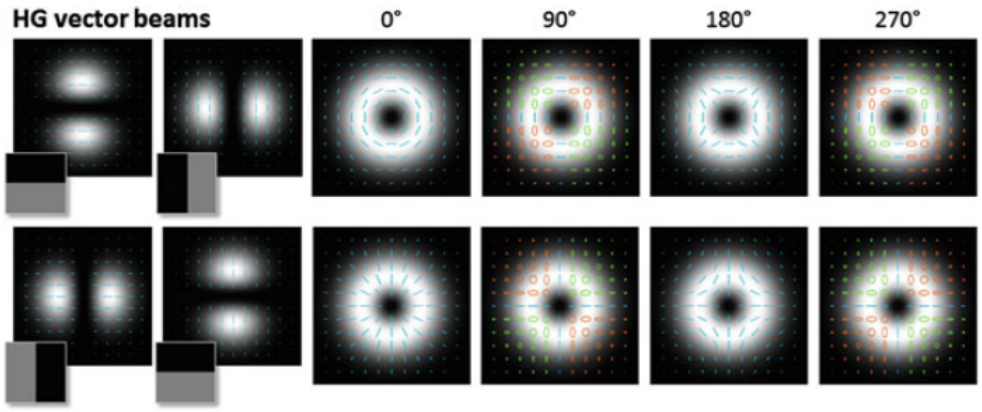

Figure 3.3: Notation:Blue-linear polarization, Orange-right elliptic polarization, Green-left elliptic.Up: Combination of HG_{01} and HG_{10} with horizontal and vertical polarization respectively. The phase ϕ is changing in each picture. Down: Combination of HG_{10} and HG_{01} with horizontal and vertical polarization respectively. The phase ϕ is changing in each picture [24]

For Laguerre-Gaussian beams, we have the expression

$$E_\omega(r,t) = \frac{1}{\sqrt{2}}(LG_{1,0}\hat{\mathbf{e}}_R + e^{i\phi}LG_{-1,0}\hat{\mathbf{e}}_L). \tag{3.31}$$

The corresponding electric field intensities in this case appear as in the following figure:

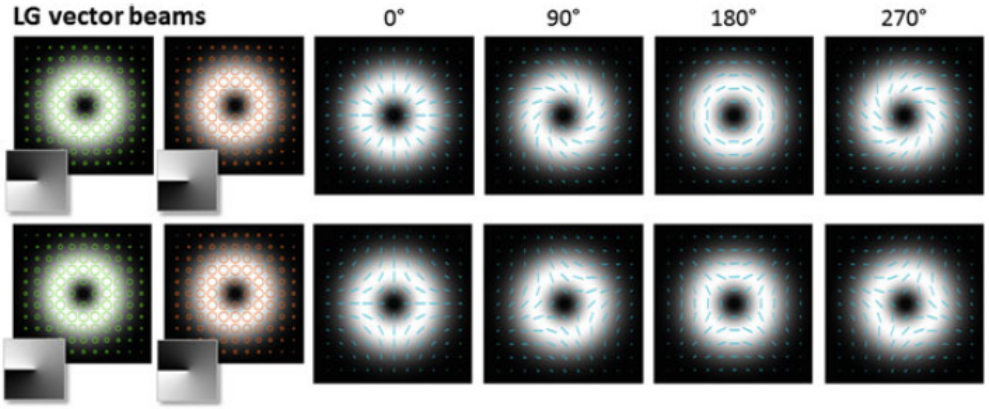

Figure 3.4: The same color notation as before.Up: Combination of LG_{10} and LG_{-10} with horizontal and vertical polarization respectively. The phase ϕ is changing in each picture. Down: Combination of LG_{-10} and LG_{10} with horizontal and vertical polarization respectively. The phase ϕ is changing in each picture [24]

In the collinear case, we have vector beams with orthogonal linear polarizations:

$$E_\omega(r,t) = \sqrt{\frac{I_0}{2}}\Big[u_{01}(r)\hat{e}_H + u_{0l_{SLM}}(r)\hat{e}_V\Big]e^{i(kz-\omega t)}. \tag{3.32}$$

However, polarization effects of the input beams are unimportant for the second harmonic generation.

3.4 Amplitude equation

We now follow [31]: In contrast to (2.37), we address transversal modes whose electric field is defined by

$$\vec{E} = \Sigma_{p,l} u^{pl}(\vec{r}) A^{pl}(z) e^{ikz}\hat{e}, \tag{3.33}$$

where

$$\begin{aligned} u^{pl}_{(n)}(\rho,\phi,z) = &\sqrt{\frac{2p!}{\pi(p+|l|)!w_n^2(z)}}\Big(\frac{\sqrt{2}\rho}{w_n(z)}\Big)^{|l|} L_p^{|l|}\Big[\frac{2\rho^2}{w_n^2(z)}\Big] \\ &\times \exp\Big[-\frac{\rho^2}{w_n^2(z)}\Big]\exp\Big[ik_n\frac{\rho^2}{2R(z)+il\phi-i\phi_{pl}(z)}\Big] \end{aligned} \tag{3.34}$$

represents an orthonormal Laguerre-Gaussian mode:

$$\int\int r dr d\phi u^{*pl}(\vec{r}) u^{p'l'}(\vec{r}) = \delta_{pp'}\delta_{ll'}. \tag{3.35}$$

Taking the time derivatives in (2.53) is time, we get expressions that are independent of time:

$$\nabla^2 E'_{h\omega} + \frac{\omega^2}{c^2}\epsilon_{h\omega}E'_{h\omega} = -\frac{\omega^2}{\epsilon_0 c^2}P'^{NL}_{h\omega}, \tag{3.36a}$$

$$\nabla^2 E'_{v\omega} + \frac{\omega^2}{c^2}\epsilon_{v\omega}E'_{v\omega} = -\frac{\omega^2}{\epsilon_0 c^2}P'^{NL}_{v\omega}, \tag{3.36b}$$

$$\nabla^2 E'_{v2\omega} + \frac{4\omega^2}{c^2}\epsilon_{v2\omega}E'_{v2\omega} = -\frac{\omega^2}{\epsilon_0 c^2}P'^{NL}_{v2\omega}, \tag{3.36c}$$

where

$$E'_{\mu} = \sum_{p,l} u^{pl}(\vec{r})A^{pl}_{\mu}(z)\exp\big(ik_\mu z\big)(\text{ incident beam}) \tag{3.37}$$

$$E'_{\mu} = \sum_{p,l} u^{pl}(\vec{r})B^{pl}_{\mu}(z)\exp\big(ik_\mu z\big)(\text{ SHG beam}) \tag{3.38}$$

h and v indicate the polarization. So μ can take on the values $h\omega, v\omega$ and $v2\omega$. We know that

$$k_\mu = \frac{\big(\epsilon_{(\omega_\mu)}\big)^{1/2}\omega_\mu}{c}. \tag{3.39}$$

and we may split ∇^2 as follows:

$$\nabla^2 = \nabla^2_\perp + \frac{\partial^2}{\partial z^2}. \tag{3.40}$$

Replacing (3.37) and (3.39) in (3.36)

$$(\nabla^2_\perp + \frac{\partial^2}{\partial z^2})[\sum_{p,l} u^{pl}(\vec{r})A^{pl}_{(\mu)}(z)\exp\big(ik_\mu z\big)] + k^2_\mu[\sum_{p,l} u^{pl}(\vec{r})A^{pl}_{(\mu)}(z)\exp\big(ik_\mu z\big)] = -\frac{\omega^2_\mu}{\epsilon_0 c^2}P'^{NL}_{\mu}. \tag{3.41}$$

The left-hand side part of the above expression reads

$$\begin{aligned}(\nabla^2_\perp + \frac{\partial^2}{\partial z^2})[\sum_{p,l} u^{pl}(\vec{r})A^{pl}_{(\mu)}(z)\exp\big(ik_\mu z\big)\exp\big(ik_\mu z\big)] + k^2_\mu[u^{pl}(\vec{r})A^{pl}_{\mu}(z)\exp\big(ik_\mu z\big)] = \\ \exp\big(ik_\mu z\big)\left[[\nabla^2_\perp u^{pl}(\vec{r})]A^{pl}_{\mu}(z) + u^{pl}(\vec{r})\left(\frac{\partial^2 A^{pl}_{(\mu)}}{\partial z^2} + 2ik_\mu\frac{\partial A^{pl}_{(\mu)}}{\partial z}\right)\right] + \\ \exp\big(ik_\mu z\big)\left[A^{pl}_{(\mu)}(z)\left(\frac{\partial^2 u^{pl}(\vec{r})}{\partial z^2} + 2ik_\mu\frac{\partial u^{pl}(\vec{r})}{\partial z}\right) + 2\frac{\partial u^{pl}(\vec{r})}{\partial z}\frac{\partial A^{pl}_{(\mu)}}{\partial z}\right].\end{aligned} \tag{3.42}$$

As we did before, we assume that the beam varies slowly along its propagation direction:

$$\left|\frac{\partial^2 u^{pl}(\vec{r})}{\partial z^2}\right| \ll k_u \left|\frac{\partial u^{pl}(\vec{r})}{\partial z}\right| \tag{3.43}$$

$$\left|\frac{\partial^2 A^{pl}_{(\mu)}(z)}{\partial z^2}\right| \ll k_u \left|\frac{\partial A^{pl}_{(\mu)}(z)}{\partial z}\right| \tag{3.44}$$

Also, we assume another approximation:

$$\left|\frac{\partial A^{pl}_{(\mu)}}{\partial z}\frac{\partial u^{pl}(\vec{r})}{\partial z}\right| \ll k_\mu \left|\frac{\partial A^{pl}_{\mu}}{\partial z}\right| \text{or } k_\mu \left|\frac{\partial u^{pl}(\vec{r})}{\partial z}\right| \tag{3.45}$$

Therefore, equation (3.41) becomes

$$\exp\big(ik_\mu z\big)\Big[A^{pl}_{(\mu)}(z)\Big(\nabla^2_\perp u^{pl}(\vec{r}) + 2ik_\mu \frac{\partial u^{pl}(\vec{r})}{\partial z}\Big) + u^{pl}(\vec{r})\Big(2ik_\mu \frac{\partial A^{pl}_{(\mu)}(z)}{\partial z}\Big)\Big] = -\frac{\omega_n^2}{\epsilon_0 c^2} P'^{NL}_{\mu} \tag{3.46}$$

We notice that

$$\nabla^2_\perp u^{pl}(\vec{r}) + 2ik_\mu \frac{\partial u^{pl}(\vec{r})}{\partial z} = 0, \tag{3.47}$$

is the solution of the Helmholtz equation for Laguerre-Gaussian modes. Finally, the expression turns into

$$u^{pl}(\vec{r})\left(2ik_\mu \frac{\partial A^{pl}_{(\mu)}(z)}{\partial z}\right) = -\frac{\omega_n^2}{\epsilon_0 c^2} P'^{NL}_{\mu} \exp\big(-ik_\mu z\big) \tag{3.48}$$

Similarly, we get:

$$u^{pl}(\vec{r})\left(2ik_\mu \frac{\partial B^{pl}_{(\mu)}(z)}{\partial z}\right) = -\frac{\omega_n^2}{\epsilon_0 c^2} P'^{NL}_{\mu} \exp\big(-ik_\mu z\big). \tag{3.49}$$

From (2.43) and (3.37), we have

$$P'^{NL}_{v2\omega} = \epsilon_0\chi^{(2)}E'_{v\omega}E'_{h\omega} = \epsilon_0\chi^{(2)}\sum_{q,r}\sum_{g,h}u^{qr}(\vec{r})A^{qr}_{(v\omega)}(z)u^{pl}(\vec{r})A^{gh}_{(v2\omega)}(z)\exp\big(i(k_{h\omega}+k_{v\omega})z\big) \tag{3.50a}$$

$$P'^{NL}_{h\omega} = \epsilon_0\chi^{(2)}E'^{*}_{v\omega}E'_{v2\omega} = \epsilon_0\chi^{(2)}\sum_{p,l}\sum_{q,r}u^{qr}(\vec{r})A^{*qr}_{v\omega}(z)u^{pl}(\vec{r})B^{pl}_{(v2\omega)}(z)\exp\big(i(k_{v2\omega}-k_{v\omega})z\big), \tag{3.50b}$$

$$P'^{NL}_{v\omega} = \epsilon_0\chi^{(2)}E'^{*}_{h\omega}E'_{v2\omega} = \epsilon_0\chi^{(2)}\sum_{p,l}\sum_{g,h}u^{gh}(\vec{r})A^{*gh}_{h\omega}(z)u^{pl}(\vec{r})B^{pl}_{(v2\omega)}(z)\exp\big(i(k_{v2\omega}-k_{h\omega})z\big), \tag{3.50c}$$

Inserting (3.50b),(3.50c) and (3.50a) in each case of (3.48) and (3.4), we obtain:

$$\frac{\partial B^{pl}_{v2\omega}}{\partial z} = \sum_{q,r}\sum_{g,h}\frac{i(2\omega)^2\chi^{(2)}}{2k_{v2\omega}c^2}\big(\Lambda^{lrh}_{pqg}(z)\big)^{*}A^{qr}_{h\omega}(z)A^{gh}_{v\omega}e^{i\Delta kz} \tag{3.51a}$$

$$\frac{\partial A^{qr}_{\omega}}{\partial z} = \sum_{p,l}\sum_{g,h}\frac{i(\omega)^2\chi^{(2)}}{2k_{v2\omega}c^2}\big(\Lambda^{lrh}_{pqg}(z)\big)B^{pl}_{(v2\omega)}(z)A^{*gh}(z)e^{-i\Delta kz}, \tag{3.51b}$$

$$\frac{\partial A^{gh}_{\omega}}{\partial z} = \sum_{p,l}\sum_{q,r}\frac{i(\omega)^2\chi^{(2)}}{2k_{v2\omega}c^2}\big(\Lambda^{lrh}_{pqg}(z)\big)B^{pl}_{(v2\omega)}(z)A^{*qr}_{h\omega}(z)e^{-i\Delta kz}, \tag{3.51c}$$

and the phase matching condition:

$$\Delta k = k_{v2\omega} - k_{h\omega} - k_{v\omega}, \tag{3.52}$$

where Λ^{lrh}_{pqg} is called overlap integral and imposes the orbital angular momentum conservation condition $l = r + h$ [25].

$$\Lambda^{lrh}_{pqg}(z) = \int\int u^{pl}_{n}(\vec{r})u^{*gh}_{o}(\vec{r})u^{*qr}_{m}(\vec{r})\,rdrd\phi \tag{3.53}$$

3.5 Experiment

3.5.1 Structured light

Interference patterns, such as the one shown in figure 3.5, contain information about intensity and phase. In order to obtain optical vortices, we prepare the screen of a spatial light modulator with the desired pattern, for which we can use a computer. Then, we send a Gaussian beam towards the screen, which by reflection generates the desired transversal mode. This process leads to the production of structured

light. This is the method that we use to generate Laguerre-Gaussian modes of arbitrary topological charge.

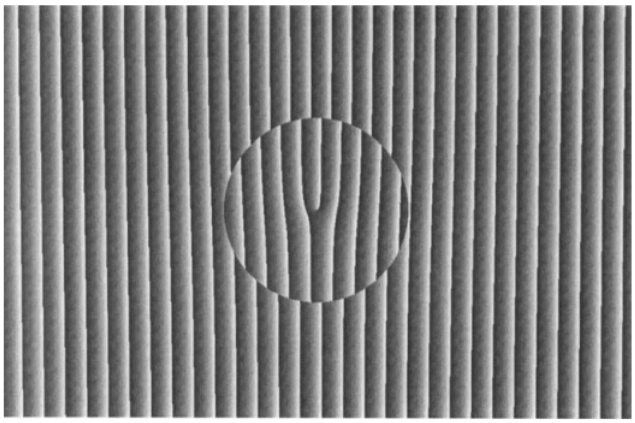

Figure 3.5: Interference pattern that contains information of a Laguerre-Gaussian mode with topological charge and radial charge equal to 1 [26]

3.5.2 SLM

The spatial light modulator (SLM) is an instrument that changes the phase and the amplitude of a transversal mode. In our experiment, we use structured light in order to transform the wavefront of the beams. The interference patterns were simulated in LabVIEW so as to obtain Laguerre-Gaussian modes. We the help of LabVIEW we could control the topological charge of each beam produced.

Our SLM is a Hamamatsu LCOS0500325 model based on the technology of liquid crystals in silicon. The liquid crystal is divided in pixels that can be addressed through a direct voltage. Thus, each pixel is oriented in order to produce a holographic pattern and transform the wavefront of the beam as we see in figure 3.6. Detailed information about the structure of the SLM can be found in Ref. [27].

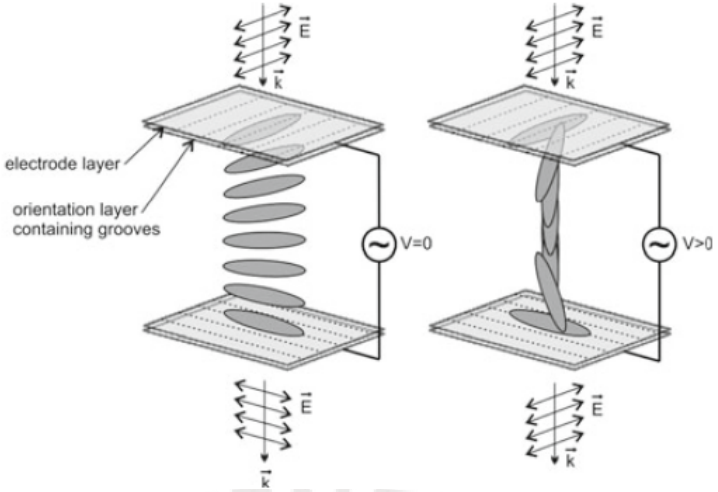

Figure 3.6: The aligment of the pixels in a SLM depends on the amount of voltage applied [27]

3.5.3 Experimental setup

The experiment is sketched in figure 3.7. The infrared laser at 1064 nm wavelength passes through a polarized beam splitter (PBS) which sets its polarization horizontally. The amount of horizontally polarized intensity is controlled by a half wave plate(HWP). The beam splits in two beams by means of a 50/50 beam splitter. One beam goes to a SLM that is controlled, as mentioned above, by a program with holographic patterns. The SLM allows us to change the topological charge l_{SLM} of the beam ψ_{SLM}. The other beam ψ_{Mask} goes to a holographic mask that has a fixed topological charge $l_{Mask} = 1$. Both beams are selected by two iris diaphragms.
One of the beams(ψ_{SLM}) changes its polarization to vertical with a HWP set at 45°. The two orthogonal polarized beams are then sent to a polarized beam-splitter (PBS-2). Before interacting with the nonlinear material, the polarization of the recombined beams is controlled by a half wave plate(HWP-3). In order to achieve phase matching, a lens focusses the beams in a potassium titanyl phosphate(KTP), which is prepared for type II phase matching and so it generates the second harmonic from 1064nm to 532nm. A dichroic mirror helps to eliminate the infrared beam. At the end of the experiment, the green beam generated is converted with a tilted lens in a Hermite-Gaussian mode in order to read off in the CCD image the resultant topological charge [34]. For more details, see [25]

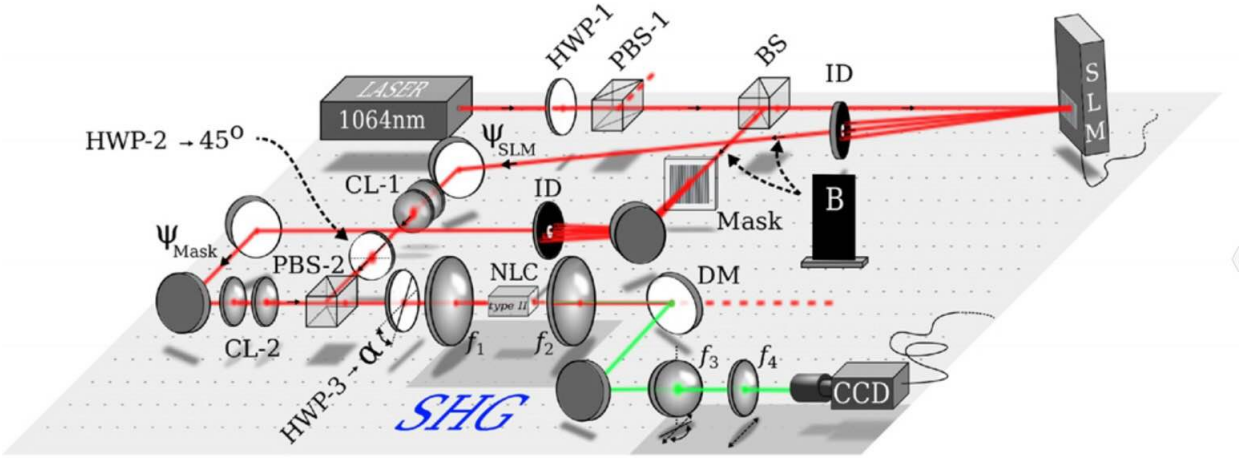

Figure 3.7: Experimental array for the second harmonic generation in collinear beams [25]

3.6 Results

The experiment yielded results that depended on the orientation of the third HWP. At 0°, the topological charge of each beam, ψ_{mask} or ψ_{SLM}, is doubled in the topological charge that was produced in second harmonic generation. At 45°the topological charges of both beams, ψ_{mask} and ψ_{SLM}, are added in the topological charge produced in second harmonic generation. Additional details of this description can be found in 3.8, where the initial topological charge of ψ_{mask} and ψ_{SLM} were 1 and 2, respectively. In order to calculate the topological charge in the picture, we need to count the diagonal black lines between the bright spots: the topological charge equals the number of bright spots minus one. Therefore, in a) and b) we count 2 and 4 black diagonal lines caused by the duplication of ψ_{mask} and ψ_{SLM}, and we count 3 in c) caused by the addition of both topological charges.

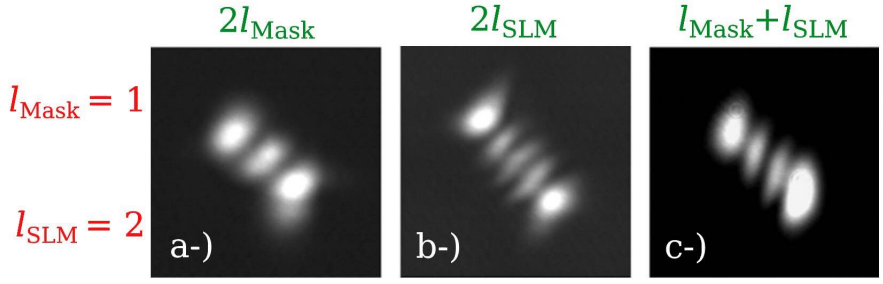

Figure 3.8: Topological charges generated in the second harmonic generation in collinear beams [25]

Chapter 4

Non-collinear interaction of Laguerre-Gaussian modes in second harmonic generation

In this chapter, we explain in detail the theoretical model of our experiment. As we shall see later, our experimental results can be explained very accurately with this model.

4.1 Amplitude equation

Similarly to the former cases, the electric field is given by a transversal function, plus polarization and propagation direction:

$$\mathbf{E}_\omega(\mathbf{r}) = \mathcal{E}_1(\mathbf{r})\hat{\mathbf{e}}_1 e^{ik_1.r} + \mathcal{E}_2(\mathbf{r})\hat{\mathbf{e}}_2 e^{ik_2.r} \tag{4.1}$$

Unit vectors are given by

$$\hat{\mathbf{e}}_1 = \cos\theta\cos\phi_1\hat{\mathbf{x}} + \sin\theta\,\hat{\mathbf{y}} + \cos\theta\sin\phi_1\hat{\mathbf{z}} \tag{4.2}$$

$$\hat{\mathbf{e}}_2 = -\sin\theta\cos\phi_2\hat{\mathbf{x}} + \cos\theta\,\hat{\mathbf{y}} + \sin\theta\sin\phi_2\hat{\mathbf{z}} \tag{4.3}$$

Here, θ is twice the angular value at which the HWP is set and ϕ the angular separation between the two beams. The transversal modes $\mathcal{E}_1(\mathbf{r})$ and $\mathcal{E}_2(\mathbf{r})$ are Laguerre-Gaussian modes with topological charges l_1 and l_2, both of them with

vanishing radial charge.

$$\begin{aligned}\mathcal{E}_1(\mathbf{r},z) &= A_1 u_{0l_1}(\mathbf{r},z),\\ \mathcal{E}_2(\mathbf{r},z) &= A_2 u_{0l_2}(\mathbf{r},z),\end{aligned} \tag{4.4}$$

We can thus write

$$u_{pl}(\mathbf{r},z) = \sqrt{\frac{2}{\pi}}\frac{\mathcal{N}_{pl}}{w(z)}\left(\frac{\sqrt{2}r}{w(z)}\right)^{|l|} L_p^{|l|}\left(\frac{2r^2}{w^2(z)}\right) e^{-[\frac{r}{w(z)}]^2} e^{i[\frac{kr^2}{2R(z)} - (2p+|l|+1)\arctan\left(\frac{z}{z_R}\right)]+l\theta]} \tag{4.5}$$

where

$$w(z) = w\sqrt{1+\left(\frac{z}{z_R}\right)^2}, \tag{4.6}$$

$$R(z) = z\left[1+\left(\frac{z_R}{z}\right)^2\right]. \tag{4.7}$$

$R(z)$ and $w(z)$ represent the radius of the wave front and the waist of the beam, respectively.

Expanding 4.1 and grouping $\hat{x}$, $\hat{y}$ and $\hat{z}$

$$\begin{aligned}\mathbf{E}_\omega(\mathbf{r}) = [&\cos\theta\cos\phi_1\mathcal{E}_1(\mathbf{r})e^{i\mathbf{k}_1.r} - \sin\theta\cos\phi_2\mathcal{E}_2(\mathbf{r})e^{i\mathbf{k}_2.r}]\hat{\mathbf{x}}\\ &+[\sin\theta\mathcal{E}_1(\mathbf{r})e^{i\mathbf{k}_1.r} + \cos\theta\mathcal{E}_2(\mathbf{r})e^{i\mathbf{k}_2.r}]\hat{\mathbf{y}}\\ &+[\cos\theta\sin\phi_1\mathcal{E}_1(\mathbf{r})e^{i\mathbf{k}_1.r} + \sin\theta\sin\phi_2\mathcal{E}_2(\mathbf{r})e^{i\mathbf{k}_2.r}]\hat{\mathbf{z}}.\end{aligned} \tag{4.8}$$

As we are dealing with type II second harmonic generation, we only consider the components x and y when applying (2.53). The second-harmonic process couples these two components with the y component of the second harmonic field. Moreover, we take both ϕ_1 and ϕ_2 close to zero, see figure 5.3. This makes the contribution from the z-component vanishingly small, see above equation.
To solve system (2.53), we thus consider three sources:

$$\begin{aligned}\mathbf{P}^{(2)}_{2\omega}(2\mathbf{k}_1) &= \frac{\chi}{2}\sin 2\theta\mathcal{E}_1^2(\mathbf{r})e^{i2\mathbf{k}_1.r}\hat{\mathbf{y}},\\ \mathbf{P}^{(2)}_{2\omega}(2\mathbf{k}_2) &= -\frac{\chi}{2}\sin 2\theta\mathcal{E}_2^2(\mathbf{r})e^{i2\mathbf{k}_2.r}\hat{\mathbf{y}},\\ \mathbf{P}^{(2)}_{2\omega}(\mathbf{k}_1+\mathbf{k}_2) &= \chi\cos 2\theta\mathcal{E}_1(\mathbf{r})\mathcal{E}_2(\mathbf{r})e^{i(\mathbf{k}_1+\mathbf{k}_2).r}\hat{\mathbf{y}},\end{aligned} \tag{4.9}$$

These sources are responsible for the generation of three electric fields in the second harmonic process. When we set $\theta = 45°$ or $\theta = 0°$, we obtain doubling and addition

of topological charges respectively.

At values $0° < \theta < 45°$, the amplitude distribution of the three beams produced in the second harmonic generation under perfect phase matching condition($\Delta k = 0$) has the following forms:

$$\begin{aligned}
\frac{dB_{pl}^{(1)}}{dz_1} &= ig \sum_{l_1,p'} \sum_{l_1,p''} \Lambda_{pp'p''}^{ll_1 l_1} A_1^2 \\
\frac{dB_{pl}^{(2)}}{dz_2} &= ig \sum_{l_2,p'} \sum_{l_2,p''} \Lambda_{pp'p''}^{ll_2 l_2} A_2^2 \\
\frac{dB_{pl}^{(12)}}{dz_{12}} &= ig \sum_{l_1,p'} \sum_{l_2,p''} \Lambda_{pp'p''}^{ll_1 l_2} A_1 A_2,
\end{aligned} \tag{4.10}$$

and the topological charge is determined by

$$\Lambda_{pp'p''}^{ll'l"} = \frac{R_{pp'p''}^{ll'l''}}{R_{000}^{000}}, \tag{4.11}$$

which imposes, as before, angular momentum conservation $l = l' + l''$. $R_{pp'p''}^{ll'l''}$ and g are defined by the expressions:

$$g = \frac{\chi}{2c} \sqrt{\frac{2\omega^3}{n_x n_y n_{2\omega}}} R_{000}^{000} \tag{4.12}$$

$$R_{pp'p''}^{ll'l''} = \int u_{pl} \Big(u_{p'l'} \Big)^* \Big(u_{p'l''} \Big)^* d^2\mathbf{r}. \tag{4.13}$$

$n_{x,y,2\omega}$ represent refraction indices along different axes.
In our experiment, radial orders p' and p'' were set to zero.

$$\begin{aligned}
\frac{dB_{pl}^{(1)}}{dz_1} &= ig \Lambda_{p00}^{ll_1 l_1} A_1^2 \\
\frac{dB_{pl}^{(2)}}{dz_2} &= ig \Lambda_{p00}^{ll_2 l_2} A_2^2 \\
\frac{dB_{pl}^{(12)}}{dz_{12}} &= ig \Lambda_{p00}^{ll_1 l_2} A_1 A_2,
\end{aligned} \tag{4.14}$$

This condition gives us two cases for overlap integrals [29].
For $l' \cdot l'' \geq 0$

$$\Lambda_{p00}^{ll'l''} = \delta_{l,l'+l''} \begin{cases} \sqrt{\frac{\xi_x^{|l'|} \xi_x^{|l''|} (|l'|+|l''|)!}{|l'|!\,|l''|!}} & (p = 0), \\ 0 & (p > 0). \end{cases}$$

which is an expected value $p = 0$. However, for $l' \cdot l'' < 0$

$$\Lambda_{p00}^{ll'l''} = \delta_{l,l'+l''} \begin{cases} \sqrt{\frac{\xi_x^{|l'|}\xi_x^{|l''|}|l'|!\,|l''|!}{p!(p+|l'+l''|)!}} & (p \leq P), \\ 0 & (p > P). \end{cases}$$

and $P = \min(\,|l'|, |l''|)$. Thus, for example, it is possible to measure different radial charges p along the propagation of the generated beams, as can be seen in figure 4.1.

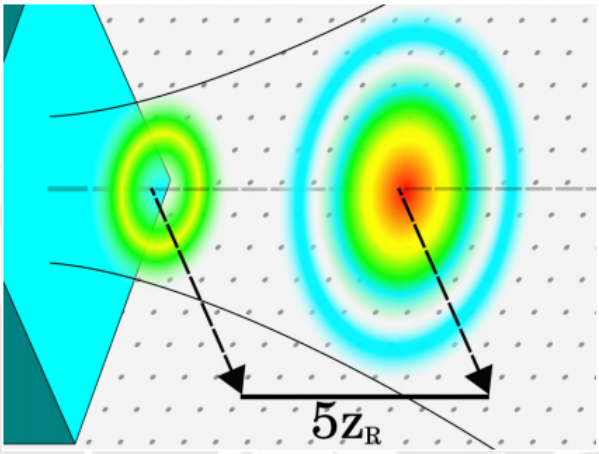

Figure 4.1: Representation of radial charges produced along the propagation of generated beams [29].

Chapter 5

Experimental setup

The setup of our experiment is sketched in figure 5.2. As before, in the experiment for collinear beams, a laser at 1064 nm(Nd: YAG laser) passes through a polarizing beam splitter which, with a half wave plate (HWP), controls the horizontal polarization of the laser. Then, a 50/50 beam-splitter divides the beam. The resulting two infrared beams reflect on two half screens of a SLM. Each part of the screen is controlled by a computer so as to manipulate the topological charge in the production of Laguerre-Gaussian modes.
One of the beams changes its polarization to vertical with a HWP rotated to 22.5°. The two orthogonally polarized beams are sent to a polarizing beam splitter. Here, since we need to control their directions, we move slightly the mirrors. If the displacement is abrupt, the second harmonic generation is not achieved because of the phase matching condition. Also, in order to modify the polarization, we set a half-wave plate before the nonlinear material (KTP). The type II phase matching is accomplished putting a convergent lens that focuses the infrared beams in the KTP. Consequently, frequency conversion from 1064nm (infrared) to 532nm (green color) is obtained. A quartz helps to deviate the infrared beam path from the green beams path. At the end of the experiment, the green beam is converted from the Laguerre-Gaussian mode to the Hermite-Gaussian mode with two tilted lenses so as to count in the CCD camera the topological charge produced in the harmonic generation.

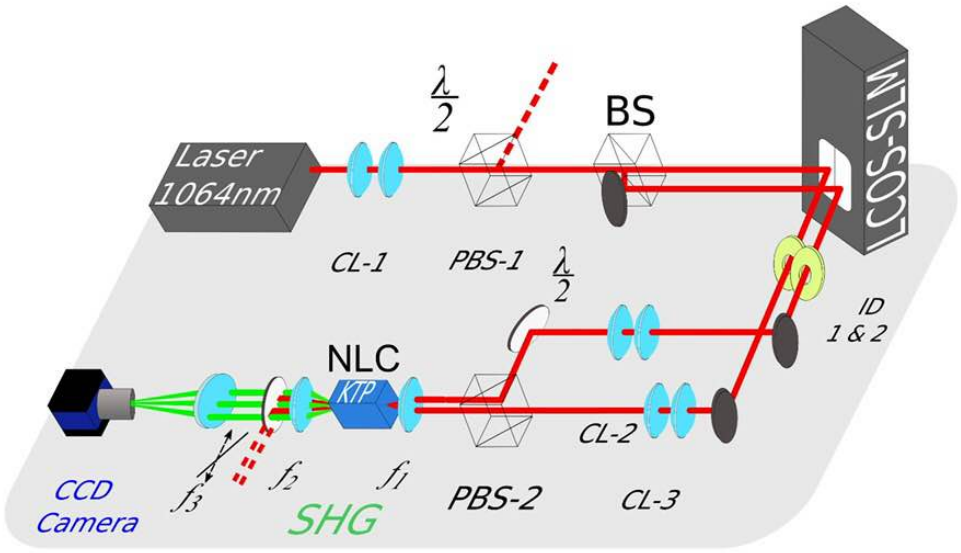

Figure 5.1: Experimental setup for the non-colinear case

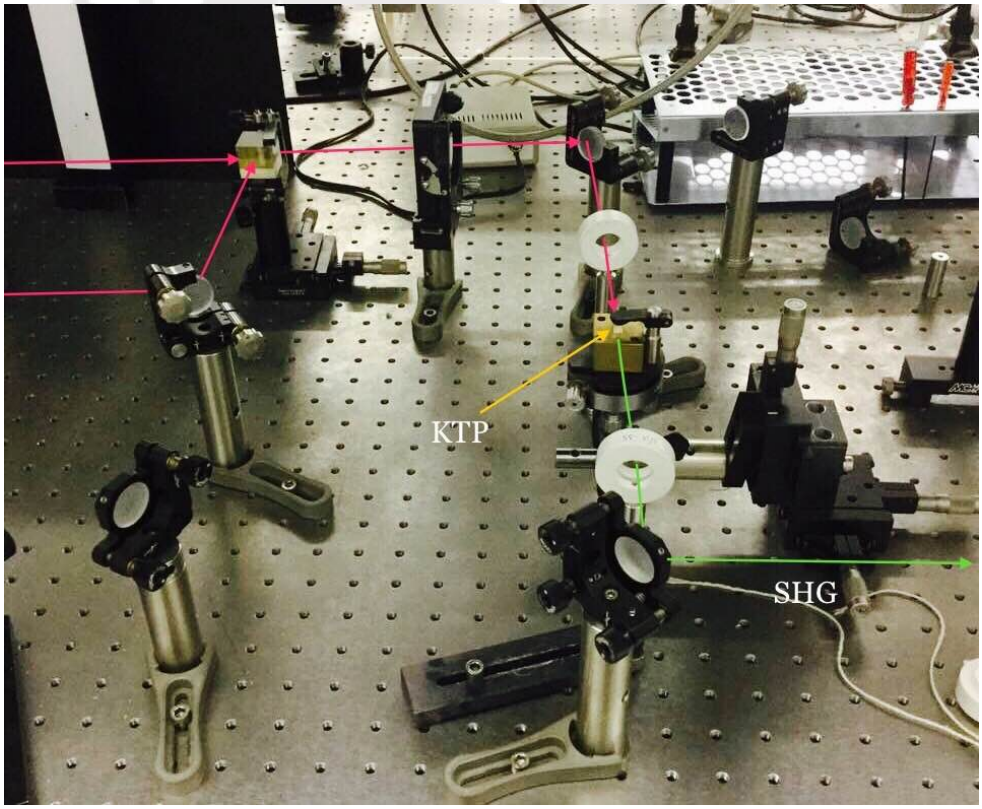

Figure 5.2: Photograph of the experimental setup for the non-collinear case. Red line and green line indicate the infrared beam path and the green beam path generated respectively

Two infrared beams pass through a type II KTP. Each one possesses three components but we just select those corresponding to x and y. Also, we adjust the setup

so as to have $\phi_1 = \phi_2$, keeping these angles close to zero. In the other way, second harmonic is not generated because of the phase matching condition.

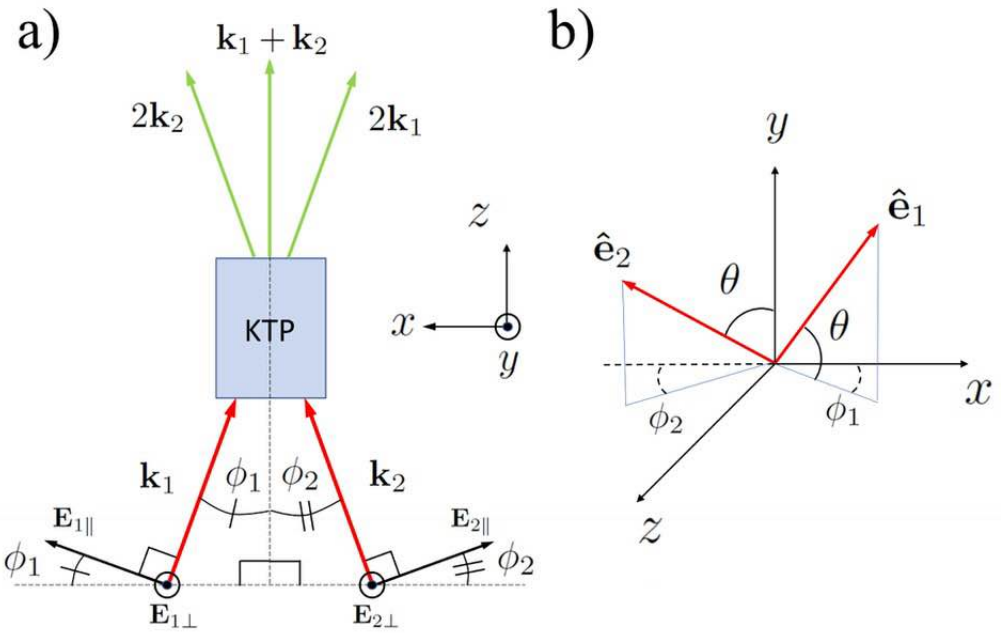

Figure 5.3: Spatial distribution of the incident beams. a)Top view of the beams. b)Tridimensional view of the beams

Chapter 6

Results

6.1 OAM operations

As we have mentioned before, in order to get our results we needed to measure the topological charge produced in the second harmony generation. To this purpose, we use a technique with a tilted lens which allowed us to count the topological charge: it is the number of bright spots minus one [34].
In figure 6.1 is sketched the output produced by the non-collinear beams when θ is between 0°and 45°. In the figure, it is possible to see the doubling topological charge produced in the non-central part of each cell, and the central spot represents the sum of the topological charges of the beams.

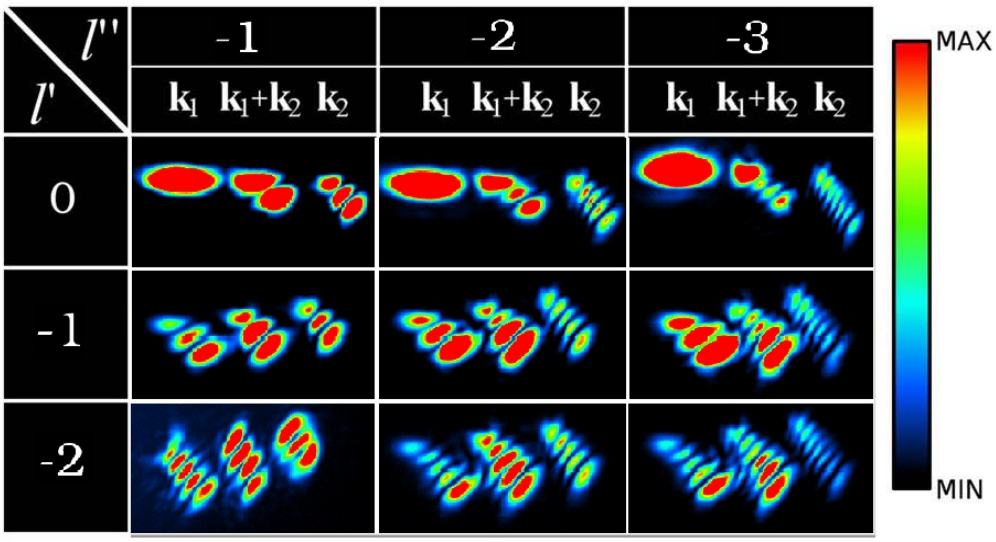

Figure 6.1: Hermitte-Gaussian spots for Laguerre-Gaussian modes with negative topological charges [28]

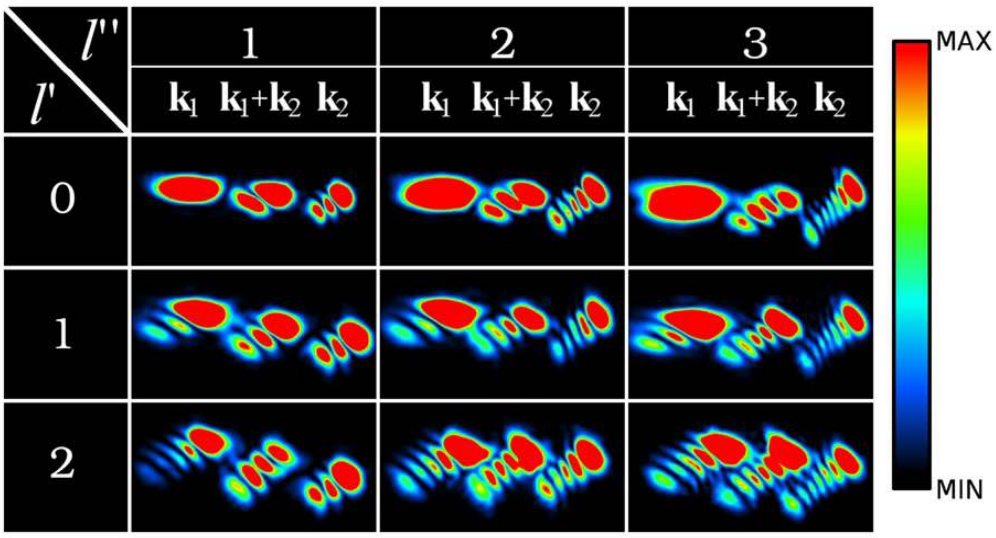

Figure 6.2: Hermitte-Gaussian spots for Laguerre-Gaussian modes with positive topological charges [28]

We see that topological charges that are greater than one cannot be clearly resolved in the figure. This is due to the energy distribution in Laguerre-Gaussian modes for higher topological charges. It is thus important to achieve good phase matching for lower topological charges, in order to get good pictures for higher topological charges.

6.2 Polarization switching

In figure 6.3, we observe two examples when $l' \cdot l'' \geq 0$ and $l' \cdot l'' < 0$. For each case, the half-wave plate is oriented going from $0°$ to $45°$ in three steps. In addition, intensity distributions for each case is shown in the right part of the picture. We can see that the intensity for each case is equally distributed among the outputs, which warns us about the conversion efficiency when generating three output beams. In part a) of figure 6.3 we have that $l' = 1$ and $l'' = -1$, then at $0°$we should see the addition of both topological charges as explained in chapter 3. However, we do not see a Gaussian beam (topological charge equals 0) in the middle. This is due to the opposite site in the operations of topological charges. Therefore, what we see is a superposition of two beams without topological charge but with radial charge 0 and 1.

On the other hand, in part b) we have negative topological charges $l' = -2$ and $l'' = -1$, so addition and doubling of topological charges happen, as described in the second paragraph.

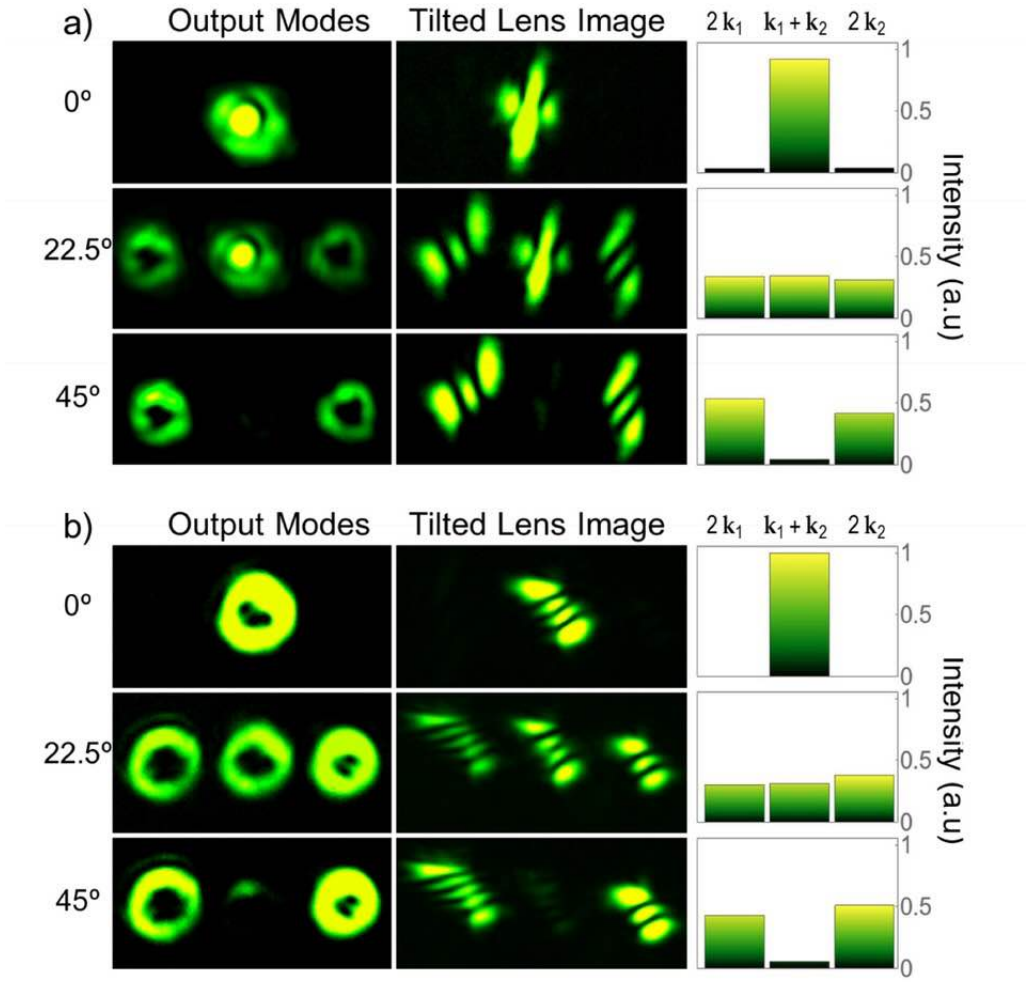

Figure 6.3: Intensity distribution of the resultant beams [28]. The equivalence transformation Laguerre-Gaussian modes(left) and Hermite-Gaussian modes(right) is shown. a)$l' = 1, l'' = -1$ b)$l' = -2, l'' = -1$. In a) it is possible to appreciate the superposition of radial charges caused by the combination of opposites topological charges [29]

6.3 Non-separability of modes in the nonlinear process

An interesting aspect appears when we describe our experiment in terms of classical entanglement [30]. Because of the non-collinear alignment, three degrees of freedom are present in the electric field, namely transversal mode, polarization and path:

$$\vec{E}_1 = u^{0l_1}(\vec{r})A^{0l_1}(z)e^{ik_1 z}\hat{e}_1 \tag{6.1}$$

$$\vec{E}_2 = u^{0l_2}(\vec{r})A^{0l_2}(z)e^{ik_2 z}\hat{e}_2, \tag{6.2}$$

where $\int \left(e^{i\mathbf{k_1}\cdot\mathbf{r}}\right)^* e^{i\mathbf{k_2}\cdot\mathbf{r}}\mathbf{d^3r} = \delta_{\mathbf{k_1},\mathbf{k_2}}$, $\hat{\mathbf{e}}^*_{\mathbf{j}} \cdot \hat{\mathbf{e}}_{\mathbf{k}} = \delta_{jk}$ and $\int u^{*0l_1}(r)u^{0l_2}(r)rdrd\theta = \delta_{l_1,l_2}$. Therefore, our input beams represent a hyper-entangled state in polarization, path and transversal mode. In mathematical terms, this means that our input is of the form

$$u_{0l_1}\hat{e}_1 + u_{0l_2}\hat{e}_2 \neq (\alpha u^{0l_1} + \beta u^{0l_2})(\gamma\hat{e}_1 + \delta\hat{e}_2) \tag{6.3}$$

However, after the second harmonic generation process, the various polarizations merge into a common one for the output beams:

$$\vec{E} = u^{0,2l_2}(\vec{r})A^{pl}(z)e^{i2k_2z}\hat{y} \tag{6.4}$$

$$\vec{E} = u^{0,l_1+l_2}(\vec{r})A^{pl}(z)e^{i(k_2+k_1)z}\hat{y} \tag{6.5}$$

$$\vec{E} = u^{0,2l_1}(\vec{r})A^{pl}(z)e^{i2k_1z}\hat{y} \tag{6.6}$$

This suggests that we can view our second harmonic experiment as a disentangling process. Although this result is not on the focus of the present thesis, it should be useful to stress this point for future research related to classical entanglement.

Chapter 7

Summary and conclusions

As we have seen in chapter 1, second harmonic generation and the appearance of orbital angular momentum in optical beams are relatively well known phenomena that nowadays have many important applications as, for instance, in gravitational wave detection [35] and communication protocols. In chapter 2, we discussed different features of the nonlinear relationship between polarization and electric fields, in particular those leading to the possibility of second harmonic generation. Then, in chapter 3, we considered the appearance of orbital angular momentum in the second harmonic and described some of our results. Chapter 4 was focused on the inclusion of a new degree of freedom: alignment of the incident beams. We presented a theoretical model that accounted for the three beams that propagate along different directions. Our results were shown and discussed in the next chapters.

In conclusion, we used polarization and alignment to produce addition and doubling of arbitrary topological charges in type II second harmonic generation. Also, by varying the orientation of a half-wave plate we observed that the three-channel output varied accordingly, from pure addition to pure doubling at 0°and 45° respectively. This outcome could be relevant for the development of communication protocols, similar to those discussed in Ref. [36].

Bibliography

[1] P. A. Franken, A. E. Hill, C. W. Peters, and G. Weinreich, *Generation of optical harmonics*, Phys. Rev. Lett. **7** (1961), 118–119.

[2] K. B. Eisenthal, *Equilibrium and dynamic processes at interfaces by second harmonic and sum frequency generation*, Annual Review of Physical Chemistry **43** (1992), 627–661.

[3] T. F. Heinz, C. K. Chen, D. Ricard, and Y. R. Shen, *Spectroscopy of molecular monolayers by resonant second-harmonic generation*, Phys. Rev. Lett. **48** (1982), 478–481.

[4] M. Han, G. Giese, and J. F. Bille, *Second harmonic generation imaging of collagen fibrils in cornea and sclera*, Opt. Express **13** (2005), 5791–5797.

[5] D. J. Brown, N. Morishige, A. Neekhra, D. S. Minckler, and J. V. Jester, *Application of second harmonic imaging microscopy to assess structural changes in optic nerve head structure ex vivo*, Journal of biomedical optics **12** (2007), 024029.

[6] J. Courtial, K. Dholakia, L. Allen, and M. J. Padgett, *Second-harmonic generation and the conservation of orbital angular momentum with high-order laguerre-gaussian modes*, Phys. Rev. A **56** (1997), 4193–4196.

[7] K. Dholakia, N. B. Simpson, M. J. Padgett, and L. Allen, *Second-harmonic generation and the orbital angular momentum of light*, Phys. Rev. A **54** (1996), R3742–R3745.

[8] M. Padgett and L. Allen, *Light with a twist in its tail*, Contemporary Physics **41** (2000), 275–285.

[9] G. Molina-Terriza, J. P. Torres, and L. Torner, *Orbital angular momentum of photons in noncollinear parametric downconversion*, Optics Communications **228** (2003), 155 – 160.

[10] F. A. Bovino, M. Braccini, M. Giardina, and C. Sibilia, *Orbital angular momentum in noncollinear second-harmonic generation by off-axis vortex beams*, JOSA B **28** (2011), 2806–2811.

[11] T. Roger, J. J. Heitz, E. M. Wright, and D. Faccio, *Non-collinear interaction of photons with orbital angular momentum*, Scientific reports **3** (2013), 3491.

[12] T. H. Maiman et al., *Stimulated optical radiation in ruby*.

[13] G. N. Lewis, D. Lipkin, and T. T. Magel, *Reversible photochemical processes in rigid media. a study of the phosphorescent state*, Journal of the American Chemical Society **63** (1941), 3005–3018.

[14] E. Hecht, *Optics*, Pearson Education, 2016.

[15] G. New, *Introduction to nonlinear optics*, Cambridge University Press, 2011.

[16] D. Kleinman, *Nonlinear dielectric polarization in optical media*, Physical Review **126** (1962), 1977.

[17] J. Midwinter and J. Warner, *The effects of phase matching method and of uniaxial crystal symmetry on the polar distribution of second-order non-linear optical polarization*, British Journal of Applied Physics **16** (1965), 1135.

[18] R. W. Boyd, *Nonlinear optics*, Academic press, 2003.

[19] M. Abramowitz and I. A. Stegun, *Handbook of mathematical functions: with formulas, graphs, and mathematical tables*, Vol. 55, Courier Corporation, 1964.

[20] F. W. Olver, *NIST handbook of mathematical functions hardback and CD-ROM*, Cambridge university press, 2010.

[21] B. E. Saleh, M. C. Teich, and B. E. Saleh, *Fundamentals of photonics*, Vol. 22, Wiley New York, 1991.

[22] L. Allen, M. W. Beijersbergen, R. Spreeuw, and J. Woerdman, *Orbital angular momentum of light and the transformation of laguerre-gaussian laser modes*, Physical Review A **45** (1992), 8185.

[23] *Department of Physics, Keio University. Sasada Lab* `http://www.phys.keio.ac.jp/guidance/labs/sasada/research/orbangmom-en.html`, April 2018.

[24] R. Fickler, *Quantum entanglement of complex structures of photons*, Springer, 2015.

[25] W. Buono, L. Moraes, J. Huguenin, C. Souza, and A. Khoury, *Arbitrary orbital angular momentum addition in second harmonic generation*, New Journal of Physics **16** (2014), 093041.

[26] J. Arlt, K. Dholakia, L. Allen, and M. Padgett, *The production of multiringed laguerre–gaussian modes by computer-generated holograms*, Journal of modern optics **45** (1998), 1231–1237.

[27] A. Jesacher, *Applications of spatial light modulators for optical trapping and image processing*, na, 2007.

[28] W. T. Buono, J. Santiago, L. J. Pereira, D. S. Tasca, K. Dechoum, and A. Z. Khoury, *Polarization-controlled orbital angular momentum switching in nonlinear wave mixing*, Opt. Lett. **43** (2018), 1439–1442.

[29] L. J. Pereira, W. T. Buono, D. S. Tasca, K. Dechoum, and A. Z. Khoury, *Orbital-angular-momentum mixing in type-ii second-harmonic generation*, Physical Review A **96** (2017), 053856.

[30] C. Borges, M. Hor-Meyll, J. Huguenin, and A. Khoury, *Bell-like inequality for the spin-orbit separability of a laser beam*, Physical Review A **82** (2010), 033833.

[31] W. T. Buono *Soma de momento angular orbital da luz na geração de segundo harmônico* Master's thesis, Universidade Federal Fluminense, Niterói, Brazil, 2017 (`https://app.uff.br/riuff/handle/1/3160`).

[32] I. Bialynicki-Birula and Z. Bialynicka-Birula, *Canonical separation of angular momentum of light into its orbital and spin parts*, Journal of Optics **13** (2011), 064014.

[33] L. Allen, M. Padgett, and M. Babiker, *IV The orbital angular momentum of light* **39** (1999), 291–372.

[34] P. Vaity, J. Banerji, and R. Singh, *Measuring the topological charge of an optical vortex by using a tilted convex lens*, Physics letters a **377** (2013), 1154–1156.

[35] S. Chelkowski, S. Hild, and A. Freise, *Prospects of higher-order laguerre-gauss modes in future gravitational wave detectors*, Physical Review D **79** (2009), 122002.

[36] R. Marchiano and J.-L. Thomas, *Doing arithmetic with nonlinear acoustic vortices*, Physical review letters **101** (2008), 064301.